AD-A098 393 NAVAL RESEARCH LAB WASHINGTON DC F/G 20/9
NUMERICAL SIMULATION OF TOKAMAK ELECTRON DYNAMICS.(U)
APR 81 W H MINER, N K WINSOR, I B BERNSTEIN AI01-76-ET-53020
UNCLASSIFIED NRL-MR-4504 NL

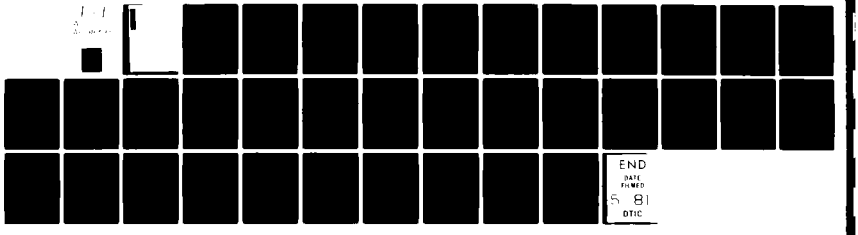

END
DATE FILMED
5 81
DTIC

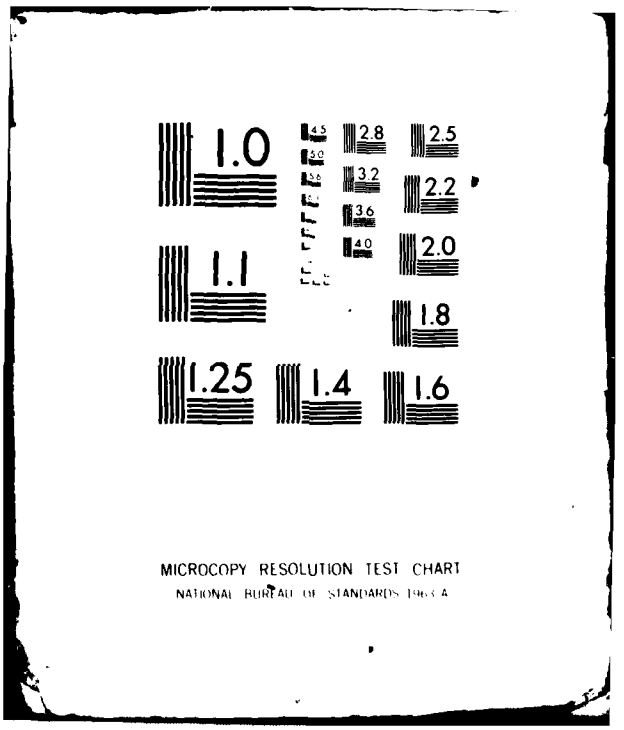
1.0
1.1
1.25
1.4
1.6
1.8
2.0
2.2
2.5
2.8
3.2
3.6
4.0
4.5
5.0
MICROCOPY RESOLUTION TEST CHART
NATIONAL BUREAU OF STANDARDS 1963 A

SECURITY CLASSIFICATION OF THIS PAGE (When Data Entered)

REPORT DOCUMENTATION PAGE

READ INSTRUCTIONS BEFORE COMPLETING FORM

1. REPORT NUMBER: NRL Memorandum Report 4504
2. GOVT ACCESSION NO.: AD-A098 393
3. RECIPIENT'S CATALOG NUMBER:

4. TITLE (and Subtitle): NUMERICAL SIMULATION OF TOKAMAK ELECTRON DYNAMICS
5. TYPE OF REPORT & PERIOD COVERED: Interim report on a continuing NRL problem.
6. PERFORMING ORG. REPORT NUMBER:

7. AUTHOR(s): W. H. Miner*, N. K. Winsor, and I. B. Bernstein**
8. CONTRACT OR GRANT NUMBER(s):

9. PERFORMING ORGANIZATION NAME AND ADDRESS: Naval Research Laboratory, Washington, DC 20375
10. PROGRAM ELEMENT, PROJECT, TASK AREA & WORK UNIT NUMBERS: ~~EX-76-A-34-1006;~~ PR 01-08; ET-53020 001; 47-0896-0-1

11. CONTROLLING OFFICE NAME AND ADDRESS: Department of Energy, Washington, DC 20545
12. REPORT DATE: April 29, 1981
13. NUMBER OF PAGES: 35

14. MONITORING AGENCY NAME & ADDRESS(if different from Controlling Office):
15. SECURITY CLASS. (of this report): UNCLASSIFIED
15a. DECLASSIFICATION/DOWNGRADING SCHEDULE:

16. DISTRIBUTION STATEMENT (of this Report)

Approved for public release; distribution unlimited.

17. DISTRIBUTION STATEMENT (of the abstract entered in Block 20, if different from Report)

18. SUPPLEMENTARY NOTES

*Present address: Science Applications, Inc., McLean, Virginia 22102
**Present address: Yale University, New Haven, Connecticut 06520

19. KEY WORDS (Continue on reverse side if necessary and identify by block number)

Tokamaks
Fokker-Planck
Electron distribution function

20. ABSTRACT (Continue on reverse side if necessary and identify by block number)

In a tokamak, the electron distribution deviates from a Maxwellian. This is because the magnetically untrapped electrons moving parallel to the applied electric field tend to run away. Because of the presence of trapped electrons, the distribution also departs from the Chapman-Enskog solution of the weak electric field problem. Previous analytic and numerical methods have treated this distortion in the limit of vanishingly small electric fields, a vanishing small number of trapped electrons, or both. We present a numerical method which relaxes these limitations, and illustrate the distribution functions which result from it.

DD FORM 1 JAN 73 1473 EDITION OF 1 NOV 65 IS OBSOLETE
S/N 0102-014-6601

SECURITY CLASSIFICATION OF THIS PAGE (When Data Entered)

TABLE OF CONTENTS

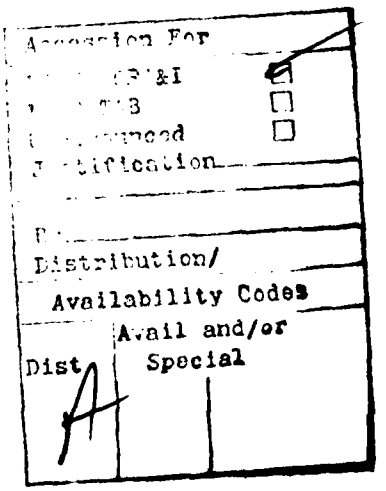

NUMERICAL SIMULATION OF TOKAMAK ELECTRON DYNAMICS

I. Introduction - Problems of Interest and History

Tokamak operation depends critically upon the physics of the electrons. The electrons transport energy, in a way still called "anomalous" after a decade of study. They determine radiation energy loss, they carry the current required for magnetohydrodynamic stability. In the absence of collisions, the dynamics of electrons trapped in local magnetic mirrors is qualitatively different from the dynamics of untrapped electrons. Electric fields and collisions then give rise to complex transport processes. In particular, an electric field parallel to the magnetic field leads to a parallel current density. For sufficiently strong electric fields, this current cannot be characterized by a quasi-steady parallel conductivity, σ. This is because the runaway electrons, which arise from the decrease of the Rutherford cross section (with increasing energy), make the conductivity depend explicity on time.

The theoretical determination of σ began with the seminal work of Chapman and Cowling,[1] and was refined by Spitzer, et al.[2] Hinton and Oberman[3] first pointed out the non-local relationship between current density and electric field in toroidal systems where the mean free path is comparable with or larger than the geometric lengths. The more recent developments are summarized by Hazeltine, et al.,[4] but all the works discussed there neglect runaway electrons.

The theory of runaway electrons was initiated by Dreicer[5] and they were first observed in toroidal geometry by W. Bernstein, et al.[6] Further analytic studies were carried out by Kruskal and I. B. Bernstein,[7] Gurevitch,[8] and Lebedev.[9] References 7-9 were complex multiple domain asymptotic analyses, the validity of which was confirmed by the numerical work of Killeen[10] and Kulsrud.[11] None of the aforementioned studies included trapped electrons.

Qualitatively, runaway behavior in even relatively weak parallel electric fields becomes important for electrons of energy a few times the thermal energy or greater. The understanding of this domain of energies was

Manuscript submitted March 11, 1981.

dramatically altered when Coppi[12] first described what he termed a "slideaway" distribution. The first associated numerical calculations were carried out by Hui.[13] The implications of the results as regards stability were discussed by Papadopoulos[14] and the resultant quasilinear diffusion further examined by Hui.[15] The application of this model to resistivity in tokamaks was presented by Winsor.[16] Elaborate numerical solutions of a model Fokker-Planck equation for times of the order of an electron-electron collision time were given by Pozolli, et al.[17]

This paper is an extension of the prior work on runaways. It is not concerned with toroidal effects and crossed field transport, but concentrates on phenomena associated with the parallel electric field. The model adopted is that of a very strong magnetic field with closed lines of force along which the magnetic field strength varies, and with an externally applied electric field parallel to it. The electrons are described by the guiding center kinetic equation with collisions represented for simplicity by the Lorentz form appropriate to electrons colliding with infinitely massive ions. This equation is presented in section II where it is written in terms of energy, magnetic moment, position on the line of force in question and time. The period of the collision-free motion of a representative electron is much less than a representative collision time. This permits reduction of the problem to consideration of a system of three bounce-averaged kinetic equations, one for trapped electrons, one for circulating electrons moving parallel to the electric field, and one for circulating electrons moving antiparallel to the electric field. The boundary conditions linking the equations are given. The details of the coefficients for a particular choice of magnetic field strength are presented in section III. A transformation of independent variables which maps the problem into a domain with rectangular boundaries is given in section IV. This lends itself to fast accurate numerical solution. The results are discussed in section V. The details of the numerical method and the calculation of the quasi-static solution are presented in Appendices A and B.

II. Kinetic Equation - Transformation to New Variables and Boundary Conditions

The guiding center distribution function $f(\underline{r}, \underline{v}; t)$ for electrons in a magnetic field is governed by the kinetic equation[18]

$$\frac{\partial f}{\partial t} + u \frac{\partial f}{\partial s} + \frac{w}{2}\left(w \frac{\partial f}{\partial u} - u \frac{\partial f}{\partial w}\right) \frac{\partial \ell n\, B}{\partial s} - \frac{e}{m} \underline{b} \cdot \underline{E} \frac{\partial f}{\partial u} = \frac{\partial f}{\partial t}\Big|_c \qquad (1)$$

Here $B = \nabla\psi \times \nabla\chi$ and E are the magnetic and electric field vectors and $\underline{b} = \underline{B}/|\underline{B}|$. In terms of the velocity $\underline{v}$ one has $u = \underline{b} \cdot \underline{v}$ and $w = |\underline{b} \times \underline{v}|$, S measures are length along $\underline{B}$, and $f = f(\psi, \chi, s, u, w, t)$ where ψ and χ are flux coordinates which label a line of force. For simplicity we neglect self collisions amongst the electrons and represent the collision term by the Lorentz collision operator[2]

$$\frac{\partial f}{\partial t}\Big|_c = \frac{2\pi n e^4 Z \ell n \Lambda}{m^2} \nabla_{\underline{v}} \cdot \left(\frac{v^2 \underline{I} - \underline{v}\,\underline{v}}{v^3} \cdot \nabla_{\underline{v}} f\right) \qquad (2)$$

$$= \nu \frac{\partial}{\partial \lambda}\left[(1-\lambda^2) \frac{\partial f}{\partial \lambda}\right] , \qquad (3)$$

which accounts accurately for small angle collisions of electrons with ions and approximately for electron-electron collisions. For electrons of speeds much greater than the rms speed, Eq. (2) is also a good representation of electron-electron collisions. Here e, m and n are the electron charge, mass and number density, Ze is the charge of the single species of ion assumed to be present, $\ell n\, \Lambda$ is the usual Coulomb logarithm,[2] $\lambda = u/v$ is the cosine of the pitch angle and the collision frequency is

$$\nu = \frac{4\pi\, n e^4\, Z \ell n \Lambda}{m^2\, v^3} . \qquad (4)$$

A transformation to energy and magnetic moment as the independent variables simplifies Eq. (1). To see this, define

$$H = \tfrac{1}{2}\, mv^2 = \tfrac{1}{2}\, m(u^2 + w^2) \qquad (5)$$

$$\mu = \tfrac{1}{2} \frac{mw^2}{B} . \qquad (6)$$

Then

$$\lambda = (1 - \mu B/H)^{\frac{1}{2}} \qquad (7)$$

and Eq. (1) is carried into

$$\frac{1}{u}\frac{\partial f}{\partial t} + \frac{\partial f}{\partial s} - e\underline{b}\cdot\underline{E}\,\frac{\partial f}{\partial H} = \frac{\partial}{\partial \mu}\left(\frac{2\nu m}{B}\,\mu u\,\frac{\partial f}{\partial \mu}\right). \tag{8}$$

where now $u = \pm\sqrt{\frac{2}{m}\,[H-\mu B]}$. Further analysis of this equation requires some knowledge of the orders of magnitude of its terms and of the magnetic geometry.

In order to model the electron dynamics in a tokamak, a magnetic geometry with closed lines of force is chosen which has a periodic variation in the field strength along the line of force. One period of the magnetic field is shown in Fig. 1. When collisions are negligible and $\underline{b}\cdot\underline{E}$ is zero, an electron with given energy H and magnetic moment μ moves on an orbit in the (u,s) phase plane as indicated schematically in Fig. 2. Note that when $H < \mu B_{max}$ the electron is trapped between maxima in the effective potential $\Phi = \mu B$ but when $H > \mu B_{max}$ the electron passes over the peak in the effective potential, the sign of u never changes, and the electron is said to be untrapped or circulating.

One can associate with each orbit a quantity

$$\tau = \int_{-\frac{L}{2}}^{\frac{L}{2}} \frac{ds}{|u|} \quad \text{(untrapped electron)}$$

$$\tau = \int_{-s_o}^{s_o} \frac{ds}{|u|} \quad \text{(trapped electron)} \tag{9}$$

For a trapped electron τ is one-half the conventional period; for an untrapped electron τ is the time required for an electron to move through one space period of B. Note that as $H \to \mu B_{max}$ the characteristic time $\tau \sim -\ell n|H - \mu B_{max}| \to \infty$.

We are concerned with situations where, for almost all values H and μ and for almost all electrons,

$$\varepsilon = \left|\tau\,\frac{\partial\, \ell n\, f}{\partial t}\right| \sim |\nu\tau| << 1 \tag{10}$$

This inequality implies that the distribution function changes in a time, determined by collisions, which is much longer than a representative period time. Let us make order of magnitude estimates of the various terms in Eq. (8).

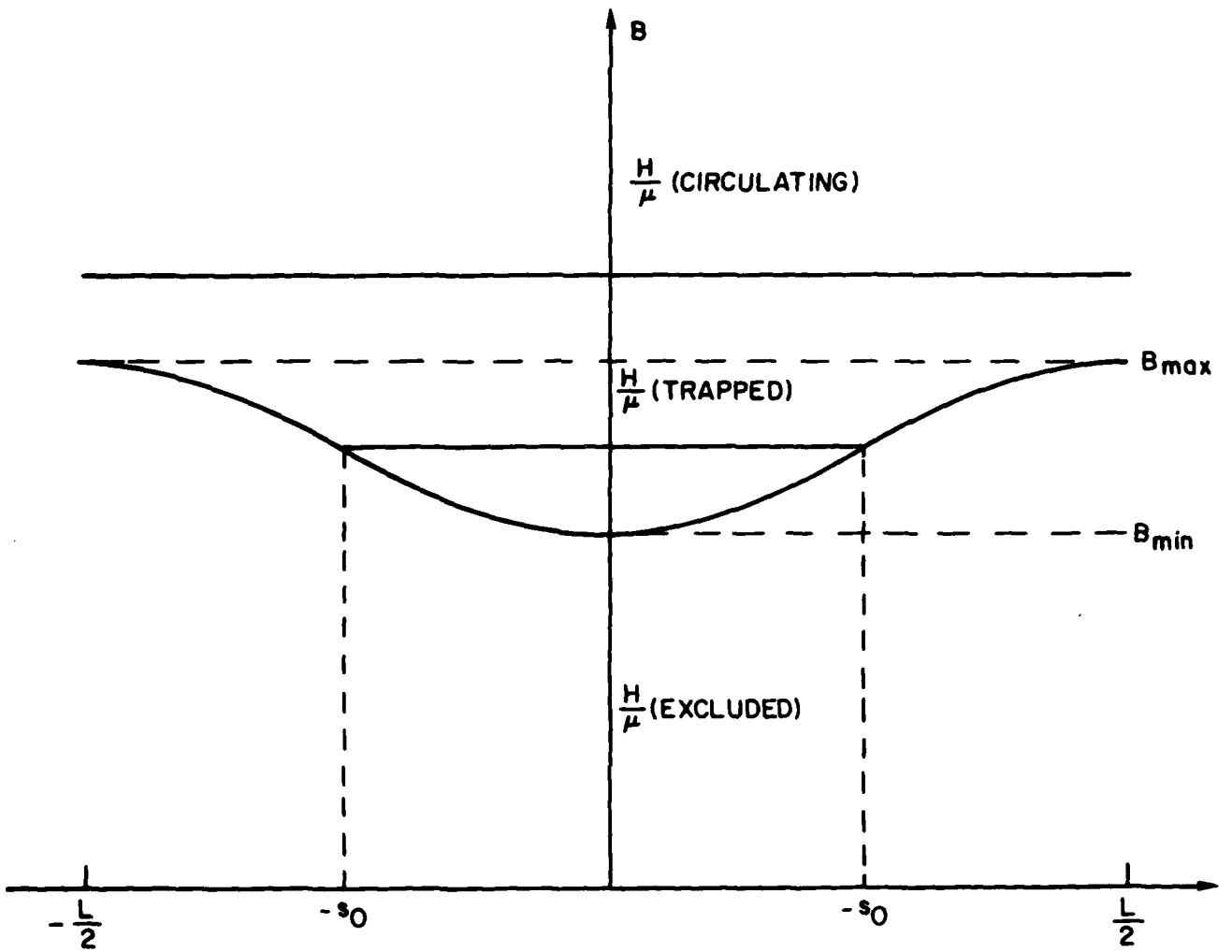

Fig. 1 - Variation of the magnitude of the magnetic field along a line of force for one field period.

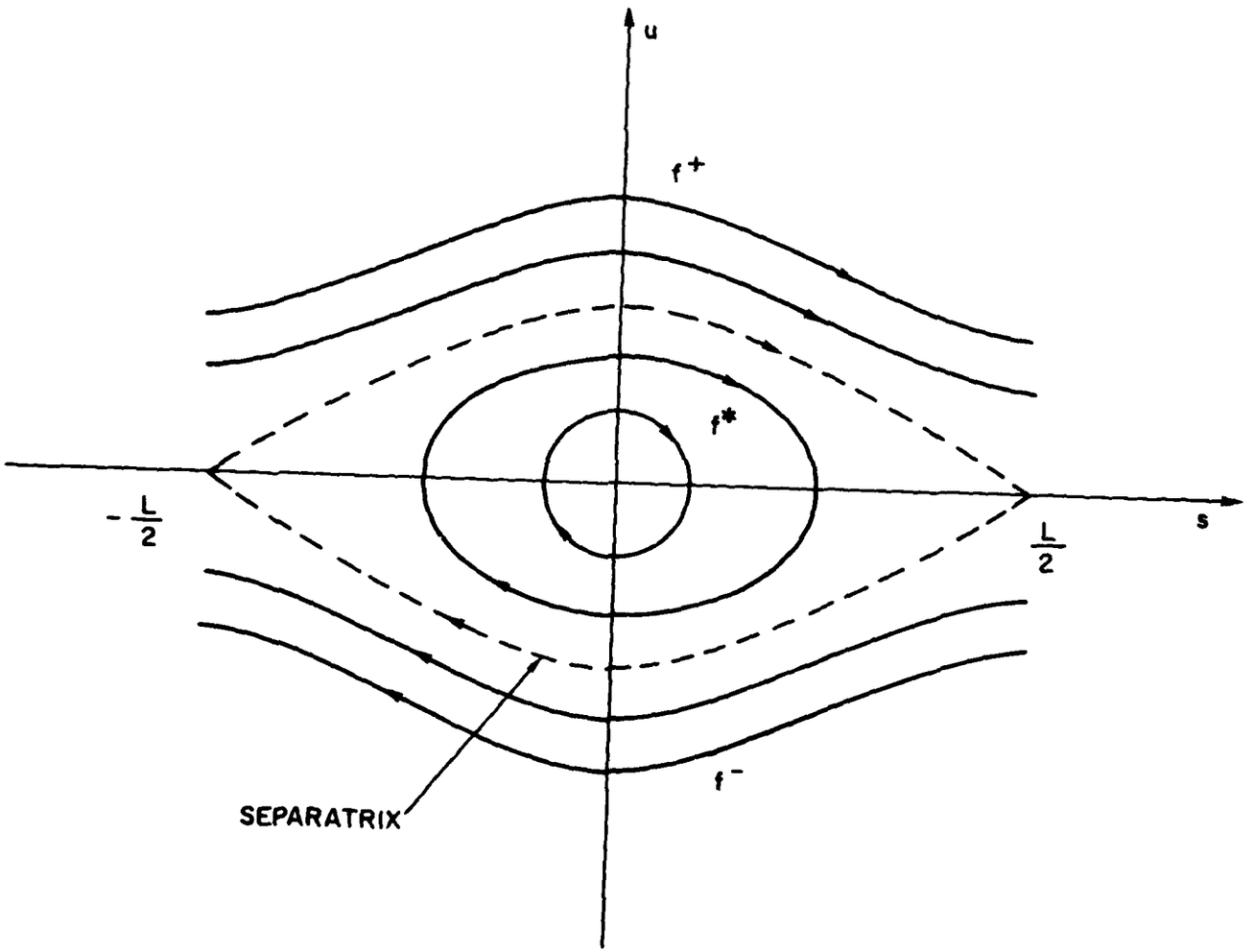

Fig. 2 - Phase space diagram, parallel velocity versus the distance along a line of force, showing the location of trapped and passing electons.

We expect smoothly-varying solutions which behave in order of magnitude like

$$\frac{L}{u}\frac{\partial f}{\partial t} \sim \tau \frac{\partial f}{\partial t} \tag{11}$$

$$L\frac{\partial f}{\partial s} \sim f \tag{12}$$

$$e\,\underline{b}\cdot\underline{E}\,L\frac{\partial f}{\partial H} \sim \frac{eEL}{H} f \tag{13}$$

and

$$\frac{\partial}{\partial \mu}\left[\frac{2\nu m}{B}\,\mu u \frac{\partial f}{\partial \mu}\right] \sim \frac{\nu}{v} f \tag{14}$$

We seek a solution of the form

$$f = f_o + f_1 + f_2 + \ldots \tag{15}$$

where in order of magnitude $|f_{m+1}/f_m| \sim \varepsilon$. Then on inserting Eq. (15) in Eq. (8) and equating like powers of ε,

$$\frac{\partial f_o}{\partial s} = 0 \tag{16}$$

$$\frac{1}{u}\frac{\partial f_o}{\partial t} + \frac{\partial f_1}{\partial s} - e\,\underline{b}\cdot\underline{E}\frac{\partial f_o}{\partial H} = \frac{\partial}{\partial \mu}\left[\frac{2\nu m}{B}\mu\frac{\partial f_o}{\partial \mu}\right] \tag{17}$$

Equation (16) requires that f_o be independent of s; e.g., $f_o = f_o(H,\mu,t)$. Henceforth we shall suppress explicit indication of ψ and χ. Thus if Eq. (17) is integrated one period around an orbit there results

$$\frac{\partial f_o}{\partial t}\oint \frac{ds}{u} - \frac{\partial f_o}{\partial H}\oint e\,\underline{b}\cdot\underline{E}\,ds = \frac{\partial}{\partial \mu}\left[\frac{\partial f_o}{\partial \mu}\oint \frac{2\nu m}{B}\mu u\,ds\right]. \tag{18}$$

The first integral on the left in (18) is τ. We choose the paths of integration as in (9) for the remaining integrals. The reason for our choice now becomes clear. The integral

$$D = \oint \frac{2\nu m}{B}\mu u\,ds \tag{19}$$

is now continuous across the separatrix.

The annihilation of the f_1 term in Eq. (17) was accomplished by integrating around a period for untrapped electrons (assuming periodicity of f_1), and around a closed orbit for trapped electrons. For untrapped electrons, the integral of the electric field term has a sign which depends on whether $\underline{u} \cdot \underline{E}$ is positive or negative: for trapped electrons, the corresponding integral vanishes.

Then Eq. (18) implies

$$\tau \frac{\partial f_o^+}{\partial t} + \Delta \frac{\partial f_o^+}{\partial H} = \frac{\partial}{\partial \mu} \left[D \frac{\partial f_o^+}{\partial \mu} \right] \tag{20}$$

$$\tau \frac{\partial f_o^-}{\partial t} - \Delta \frac{\partial f_o^-}{\partial H} = \frac{\partial}{\partial \mu} \left[D \frac{\partial f_o^-}{\partial \mu} \right] \tag{21}$$

$$\tau \frac{\partial f_o^*}{\partial t} = \frac{\partial}{\partial \mu} \left[D \frac{\partial f_o^*}{\partial \mu} \right] \tag{22}$$

and

$$\Delta = \left| e \int ds \, \underline{b} \cdot \underline{E} \right| . \tag{23}$$

where f^* denotes the distribution function of the trapped electrons, and $f^{\pm}$ that of the untrapped electrons, the $\pm$ being taken according as $\text{sgn } u = \pm \text{ sgn } \underline{b} \cdot \underline{E}$. These three parts of the electron distribution are indicated in Figs. 1 and 3. On the separatrix, or better said on adjacent points on the side of the item boundary layer straddling the separatrix in which $t \to \infty$

$$f^+ = f^- = f^* \tag{24}$$

In addition f must be regular at all the natural singular points of the differential equations. As one approaches the separatrix, where the bounce average which is used to derive Equations (20) - (22) fails, one can invoke conservation of flux across the separatrix to provide the required condition. The details are given in Appendix A.

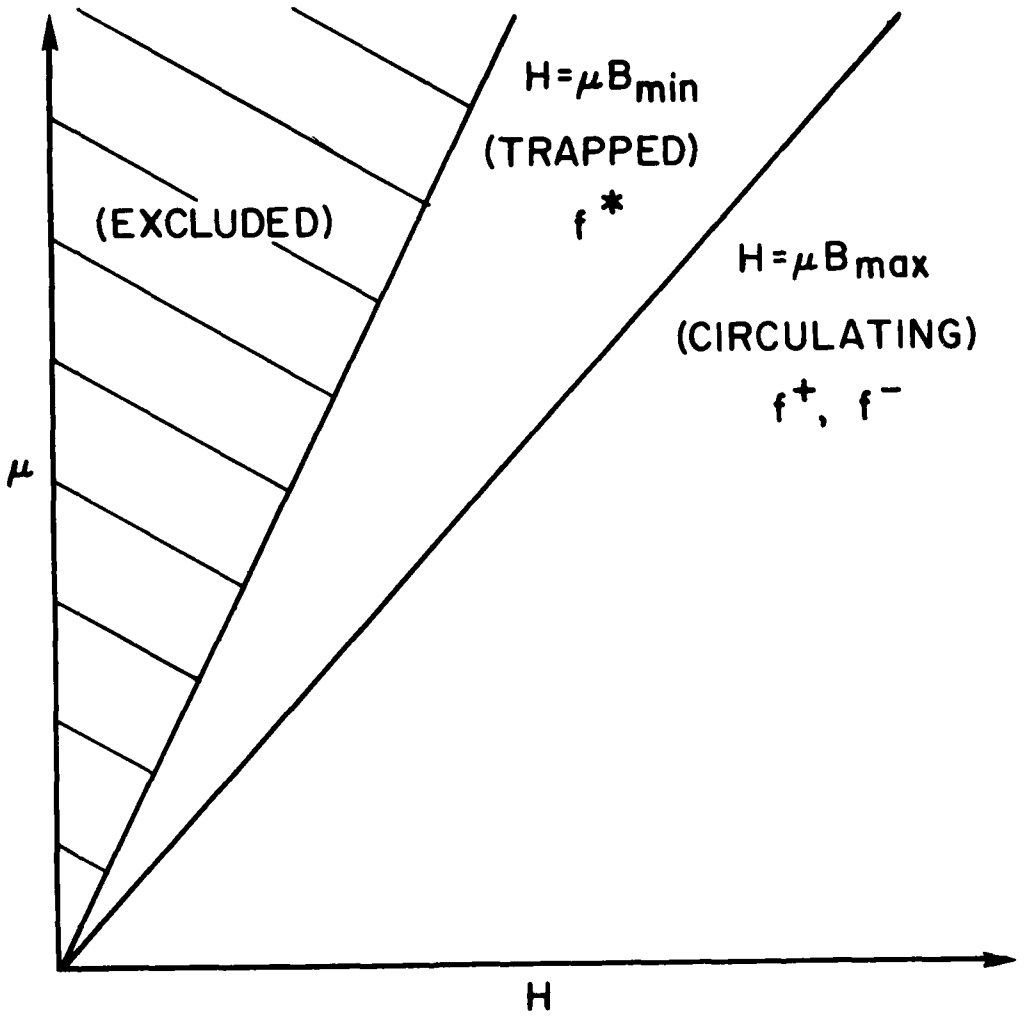

Fig. 3 - Diagram in magnetic moment versus energy space showing the location of trapped and passing electrons.

III. A Magnetic Field Geometry

The transport coefficients τ, Δ and D may be calculated when the magnetic field is known as a function of space. For simplicity, we shall assume the sinusoidal form

$$B(s) = B_{min} \{1 + \delta [1 - \cos (\frac{2\pi s}{L})]\}$$

$$= B_{min} \{1 + 2\delta \sin^2 (\frac{\pi s}{L})\} \tag{25}$$

where

$$\delta = \frac{B_{max} - B_{min}}{2 B_{min}} \tag{26}$$

This magnetic field behavior is depicted in Fig. 1. As indicated in Fig. 2, the parallel electron velocity varies with this magnetic field

$$u(s) = \{\frac{2}{m} [H - \mu B(s)]\}^{\frac{1}{2}}.$$

For trapped electrons, u vanishes at the turning point, $\pm s_o$, where

$$s_o = \frac{L}{\pi} \arcsin \left(\frac{H-\mu B_{min}}{2\delta\mu B_{min}} \right)^{\frac{1}{2}} \tag{27}$$

Now let us define

$$s_{max} = \begin{cases} L/2, & H > \mu B_{max} \\ s_o, & H \leq \mu B_{max} \end{cases}. \tag{28}$$

Then in (H, μ) coordinates

$$\tau = \frac{2L}{\pi[\frac{2}{m}(H-\mu B_{min})]^{\frac{1}{2}}} \int_o^{\frac{\pi s_{max}}{L}} [1 - \frac{2\delta\mu B_{min}}{H-\mu B_{min}} \sin^2 \theta]^{-\frac{1}{2}} d\theta \tag{29}$$

$$\Delta = \begin{cases} 2\left| \int_o^{L/2} \underline{b} \cdot \underline{E} \, ds \right|, & H > \mu B_{max} \\ 0, & H \leq \mu B_{max} \end{cases} \tag{30}$$

and

$$D = \frac{4Lm\nu\mu}{\pi B_{min}} \left[\frac{2}{m} (H-\mu B_{min}) \right]^{\frac{1}{2}} \int_0^{\frac{\pi s_{max}}{L}} \frac{\left[1- \frac{2\delta\mu B_{min}}{H-\mu B_{min}} \sin^2 \theta\right]^{\frac{1}{2}}}{1 + 2\delta \sin^2 \theta} d\theta. \qquad (31)$$

Performing the θ integrations in Equations (29) and (31) and employing the superscript notation introduced in Section II, the transport coefficients may be expressed by

$$\tau = \begin{cases} \tau^{\pm} = \alpha k K(k) & H > \mu B_{max} \\ \tau^{*} = \alpha K(1/k) & H \leq \mu B_{max} \end{cases} \qquad (32)$$

where

$$\alpha = \frac{L}{\pi \left(\frac{\delta\mu}{m} B_{min}\right)^{\frac{1}{2}}} \qquad (33)$$

$$k = \left[\frac{2\delta\mu B_{min}}{H-\mu B_{min}} \right]^{\frac{1}{2}} \qquad (34)$$

and $K(k)$ is the complete elliptic integral of the first kind defined by[19]

$$K(k) \equiv \int_0^{\frac{\pi}{2}} d\theta \, (1-k^2\sin^2\theta)^{-\frac{1}{2}} \qquad (35)$$

and

$$\Delta = \begin{cases} \Delta^{\pm} = 2 \left| e \int_0^{\frac{L}{2}} b \cdot E \, ds \right| & H > \mu B_{max} \\ \Delta^{*} = 0 & H \leq \mu B_{max} \end{cases} \qquad (36)$$

and

$$D = \begin{cases} D^{\pm} = \frac{\beta}{k} E(k) & H > \mu B_{max} \\ D^{*} = \beta[E(1/k) - (1-1/k^2)K(1/k)] & H \leq \mu B_{max} \end{cases} \qquad (37)$$

where

$$\beta = \frac{8L}{\pi} \nu\mu^{\frac{3}{2}} \left(\frac{\delta\ m}{B_{min}}\right)^{\frac{1}{2}} \tag{38}$$

and E(k) is a complete elliptic integral of the second kind defined by[19]

$$E(k) \equiv \int_0^{\frac{\pi}{2}} d\theta(1-k^2\sin^2\theta)^{\frac{1}{2}}. \tag{39}$$

For convenience, the θ variation in the denominator of the integral in Equation (31) was neglected, and therefore the expression in Equation (37) is an upper bound for the diffusion coefficient.

IV. Reduction to the Unit Square - Second Transform and Comments on Computability

The equation for the averaged distribution function, f, is in its simplest form in Eq. (18). In velocity space, it consists of purely convective "flow" in the H-direction plus purely diffusive motion in the μ-direction. This would be easy to solve either numerically or computationally, except for the boundary and matching conditions.

Extensive numerical studies have been performed on a close relative of (18), the Fokker-Planck Equation.[3,5,11,20] References 5 and 11 have not included the magnetic trapping effects, but have required special treatment near $H = 0$ and $H = \infty$. References 3 and 20 have included trapped-electron effects, and require special treatment on the separatrix. Much of this difficulty can be removed by choosing a compact coordinate system (the unit square) in which the separatrix is parallel to one of the coordinate boundaries.

This transformation may be chosen for computational convenience from the rational functions. Consider the variables

$$x = \frac{z-1}{z+a} \tag{40}$$

and

$$y = \frac{H}{H+H_o} \equiv 1 - \frac{H_o}{H+H_o} \tag{41}$$

where

$$z = \frac{H}{\mu B_{min}} . \tag{42}$$

Here a and H_o are constants which will be chosen later to scale the coordinate system for problems of interest.

Equations (21-23) when transformed assume the conservative form

$$\frac{\partial}{\partial t}\left(\frac{\tau}{J} f_o\right)+\frac{\partial}{\partial y}\left(\frac{\Delta}{J}\frac{\partial y}{\partial H} f_o\right)+\frac{\partial}{\partial x}\left(\frac{\Delta}{J}\frac{\partial x}{\partial H} f_o\right) = \left[\frac{\partial}{\partial x}\ \frac{D}{J}\left(\frac{\partial x}{\partial \mu}\right)^2 \frac{\partial f_o}{\partial x}\right] \tag{43}$$

where f_o represents f_o^+, f_o^- or f_o^* with the appropriate definitions of τ, Δ and D given in Section III.

$$\frac{\partial x}{\partial H} = \frac{1}{H_o} \frac{1-y}{y} \frac{(1-x)\ (1+ax)}{1+a} \tag{44}$$

$$\frac{\partial x}{\partial \mu} = - \frac{B_{min}}{H_o} \frac{1-y}{y} \frac{(1+ax)^2}{1+a} \tag{45}$$

$$\frac{\partial y}{\partial H} = \frac{1}{H_o} (1-y)^2 \tag{46}$$

and the Jacobian is

$$J = \frac{B_{min}}{H_o{}^2} \frac{(1-y)^3}{y} \frac{(1+ax)^2}{1+a} . \tag{47}$$

The separatrix is now along the coordinate line

$$x = x_s \equiv \frac{B_{max} - B_{min}}{B_{max} + aB_{min}} . \tag{48}$$

The cost of this simplification is a convection term with derivatives in both coordinates.

The numerical analysis of Eq. (43) is now elementary. The convection and diffusion operations can be performed on a Cartesian (x,y) grid with conventional methods.[10] The functions f_o^+ and f_o^- differ above the separatrix, and are the same (i.e., $f^+ = f^- = f^*$) below it, and are continuous on it. The boundary conditions are

$$\partial f_o / \partial y = 0 \tag{49}$$

at $x = 0$ and $x = 1$, and

$$\partial f_o / \partial x = 0 \tag{50}$$

at $y = 0$ and $y = 1$.

And the flux conservation conditioning

$$\frac{D}{J} \left(\frac{\partial x}{\partial \mu}\right)^2 \frac{\partial f_o}{\partial x}$$

continuous on $x = x_s$. If desired, the conservation condition can be relaxed, and an asymptotic form can be prescribed at $y = 1$.

This form of the model is now easy to apply to physical problems. The next sections present some applications. Appendix A describes the details of the numerical methods.

V. Conclusions

Figure 4 shows the electron distribution function, f_e, for three values of the applied electric field at the same final time. The curves are lines of constant f_e and the difference between each contour is $\Delta f_e = \exp[(\ln f_e(\max) - \ln f_e(\min)/(N_c+1)]$ where N_c is the total number of contours. For case (a), the applied electric field is so weak, $E/E_D \ll 1$, that the departure of the electron distribution function from a Maxwellian is not discernable in the graph, i.e., lines of constant f_e are semicircles. In case (b), the applied electric field is larger and the departure from Maxwellian, though small, is now evident in the plot. Finally, in case (c), the electric field has generated a large high energy tail on the distribution function and the level curves are markedly distorted from semicircles.

Figures 5 and 6 display the electron distribution function as a function of the parallel and perpendicular velocities respectively, i.e., $f_e(v_\parallel)$ and $f_e(v_\perp)$. For the small electric field case, the distribution functions remain essentially Maxwellian with equal parallel and perpendicular temperatures (the initial condition). For the case of the large electric field, $f_e(v_\parallel)$ is highly asymmetric and the increase in the perpendicular temperature is attributable to pitch-angle scattering.

Figure 7 shows the variation of the plasma resistivity, η, defined as the ratio of the current density to the parallel electric field, as a function of time for two values of the applied electric field. Each curve exhibits two different types of behavior. The first is a very rapid response to the electric field which is shown by the sharp decrease in the plasma resistivity. However, as the distribution distorts from the initial Maxwellian, the pitch-angle diffusion becomes important and a second regime is reached with a much

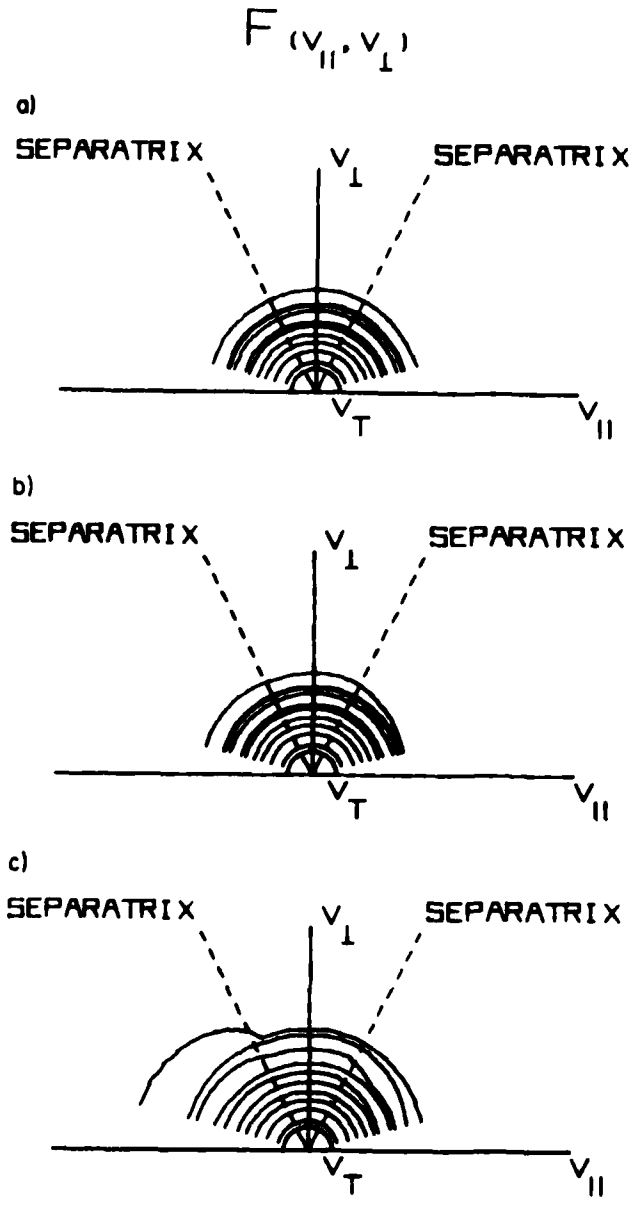

Fig. 4 - Velocity space plots of the electron distribution function for their values of the applied electric field after fifty collision times: a) E/E_D = .0085, b) E/E_D = .085, and c) E/E_D = .85.

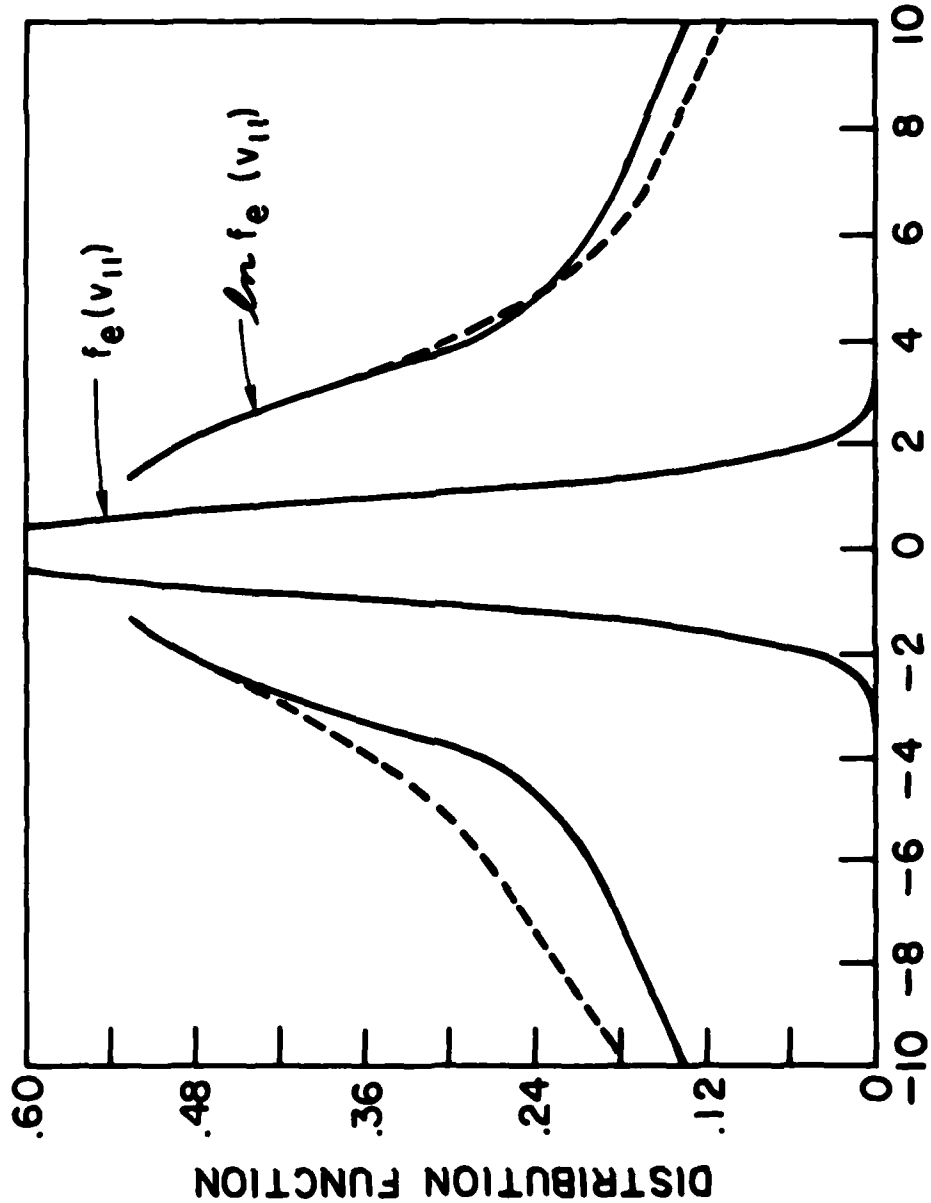

Fig. 5 - The electron distribution function as a function of the parallel velocity. The solid line represents the initial distribution and the dashed line represents the distribution after fifty collision times.

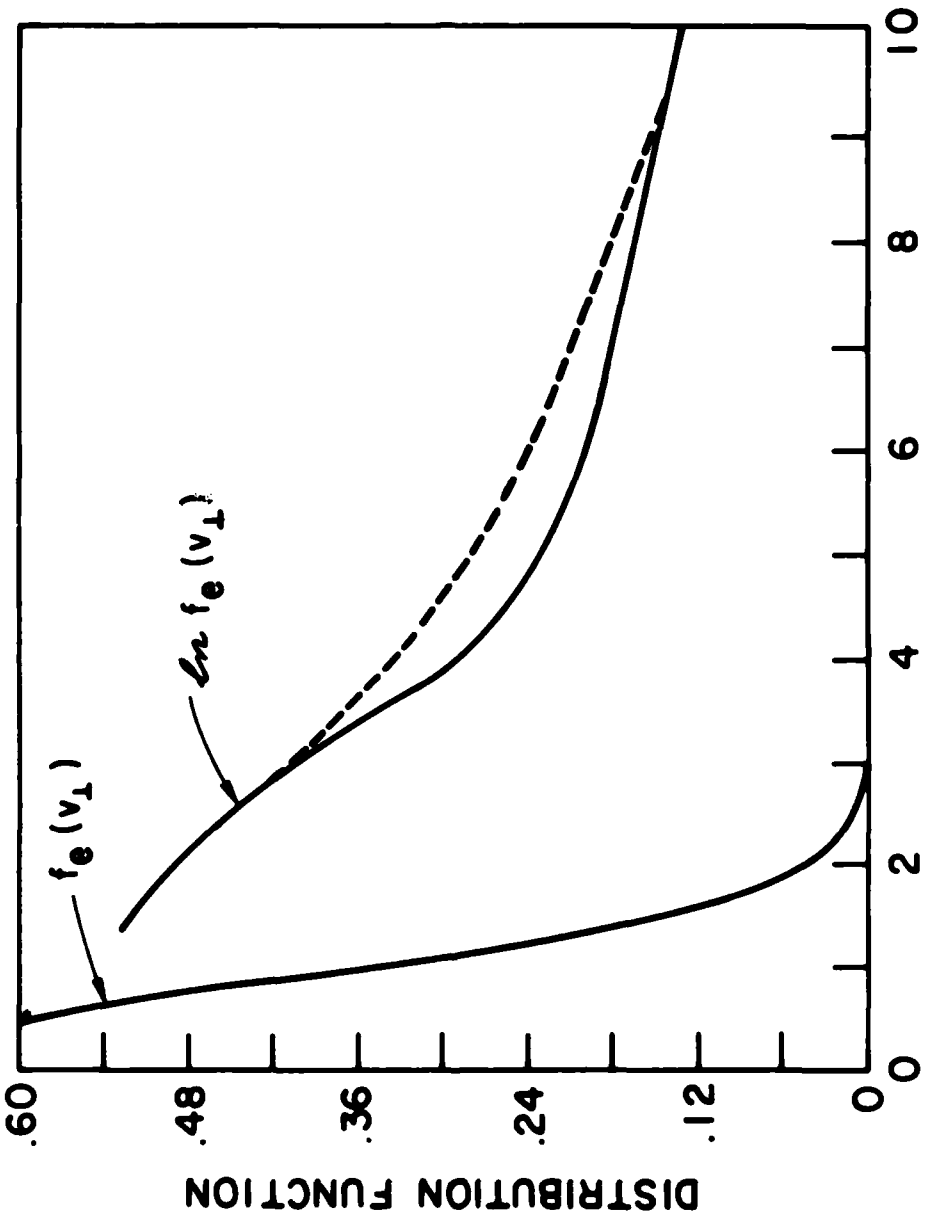

Fig. 6 - The electron distribution function as a function of the perpendicular velocity. The solid line represents the initial distribution and the dashed line represents the distribution after fifty collision times.

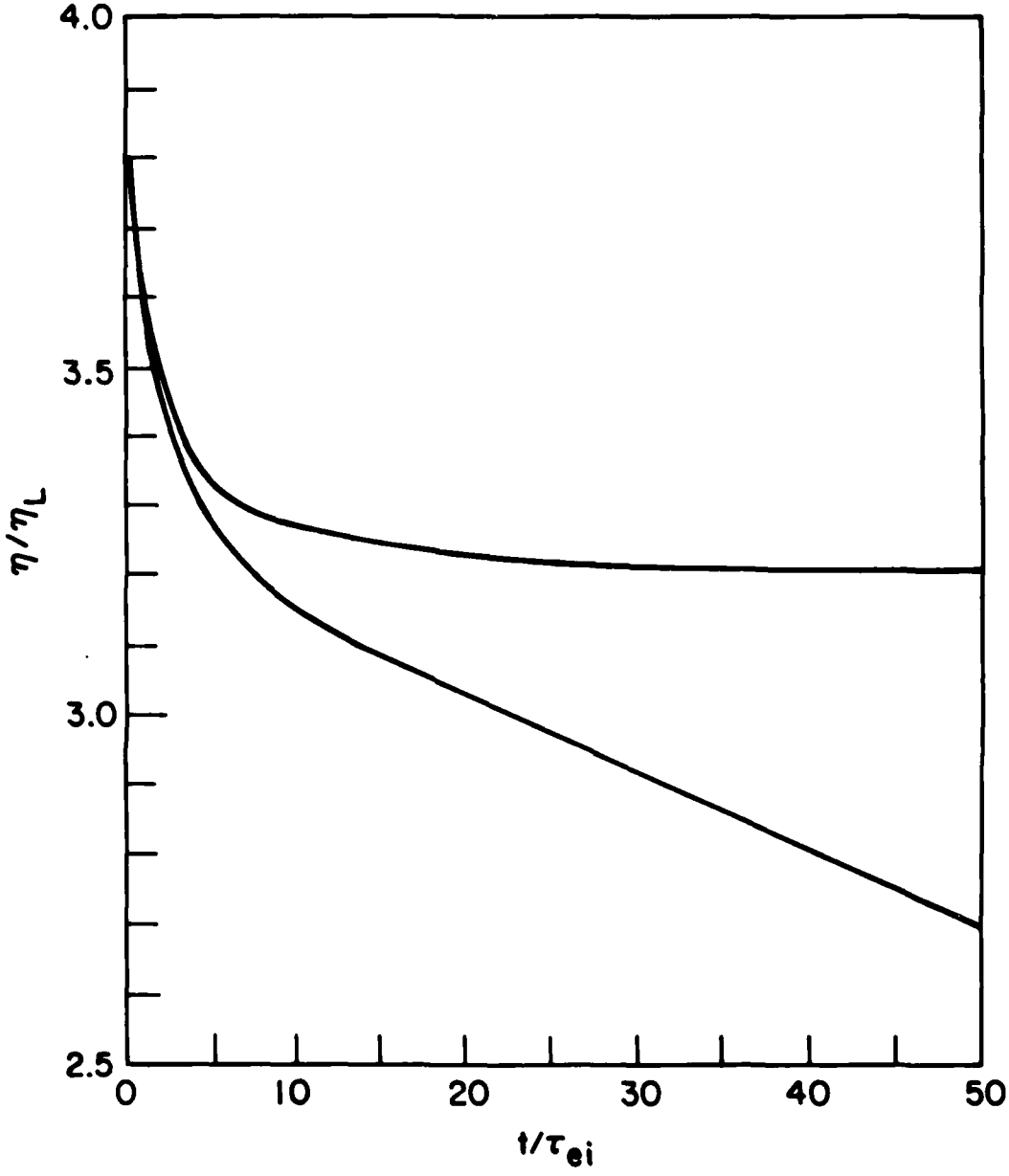

Fig. 7 - The resistivity as a function of time for two values of the applied electric field. In the upper curve E/E_D = .0085 and in the lower curve E/E_D = .85.

more slowly varying resistivity. The departure from a constant resistivity is attributed to the runaway electrons and can be seen to be present even for the small electric field case, though it sets in at ever later times as the electric field decreases.

Figures 8 and 9 display the results of varying the number of trapped particles. Figure 8 shows the electron distribution function for three values of $\delta = (\epsilon = a/R)$ at the same final time for the same applied electric field. The variation in the number of trapped particles is shown by the size of the angle subtended by the two dashed lines representing the position of the separatrix. The time evolution of the plasma resistivity corresponding to these cases are shown in Fig. 9. The important point to note here is the increase in the resistivity due to the decrease in the available current carriers, i.e., trapped particles cannot contribute to the plasma current.

Finally, Fig. 10, shows the time evolution of the plasma resistivity for three different initial electron distribution functions. The solid line represents the resistivity resulting from an initially Maxwellian distribution. The dashed line represents the resistivity when the initial distribution was that calculated in Appendix B and corresponds to the counterpart of the Spitzer-Harm calculation for the case of trapped particles. The ratio of the two asymptotic values was found to be approximately 5/3. When this factor was included, and it is believed to be a numerical error in the code, the result was the dotted line. The initial transient is believed to be associated with finite grid size effects. This shows that the Maxwellian plus the first order correction yield a much better approximation to the asmyptotic distribution than the Maxwellian alone.

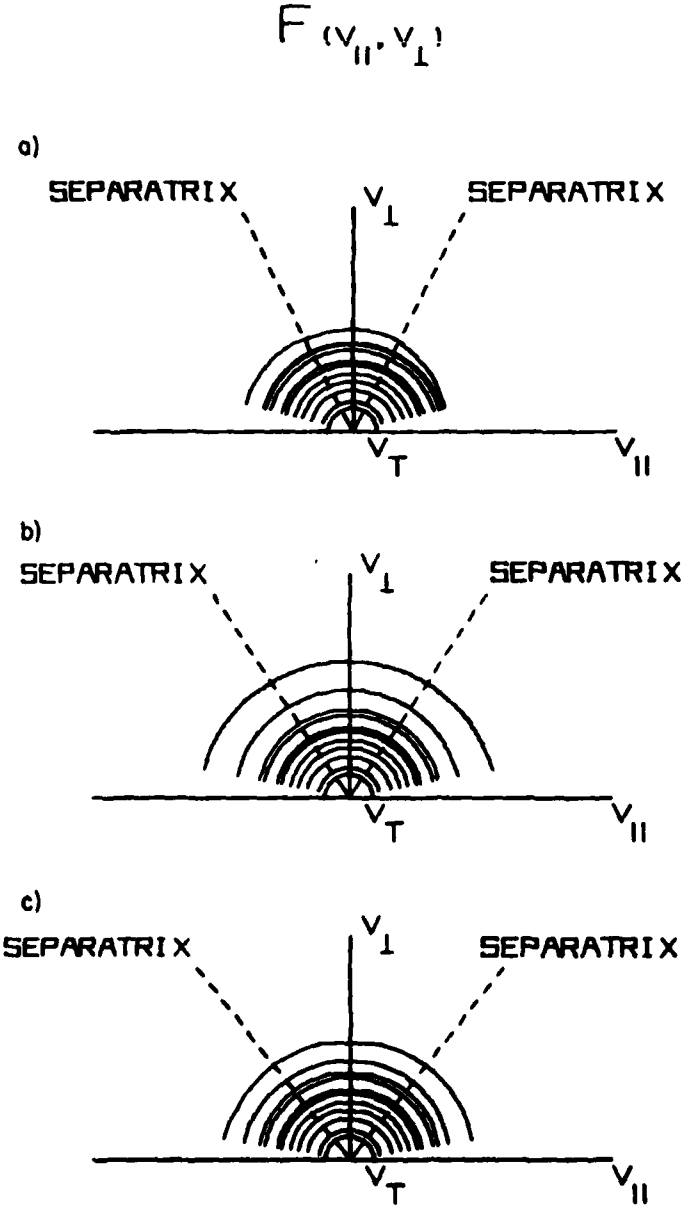

Fig. 8 - Velocity space plots of the electron distribution function for three values of δ; a) δ = .100, b) δ = .175 and c) δ = .250

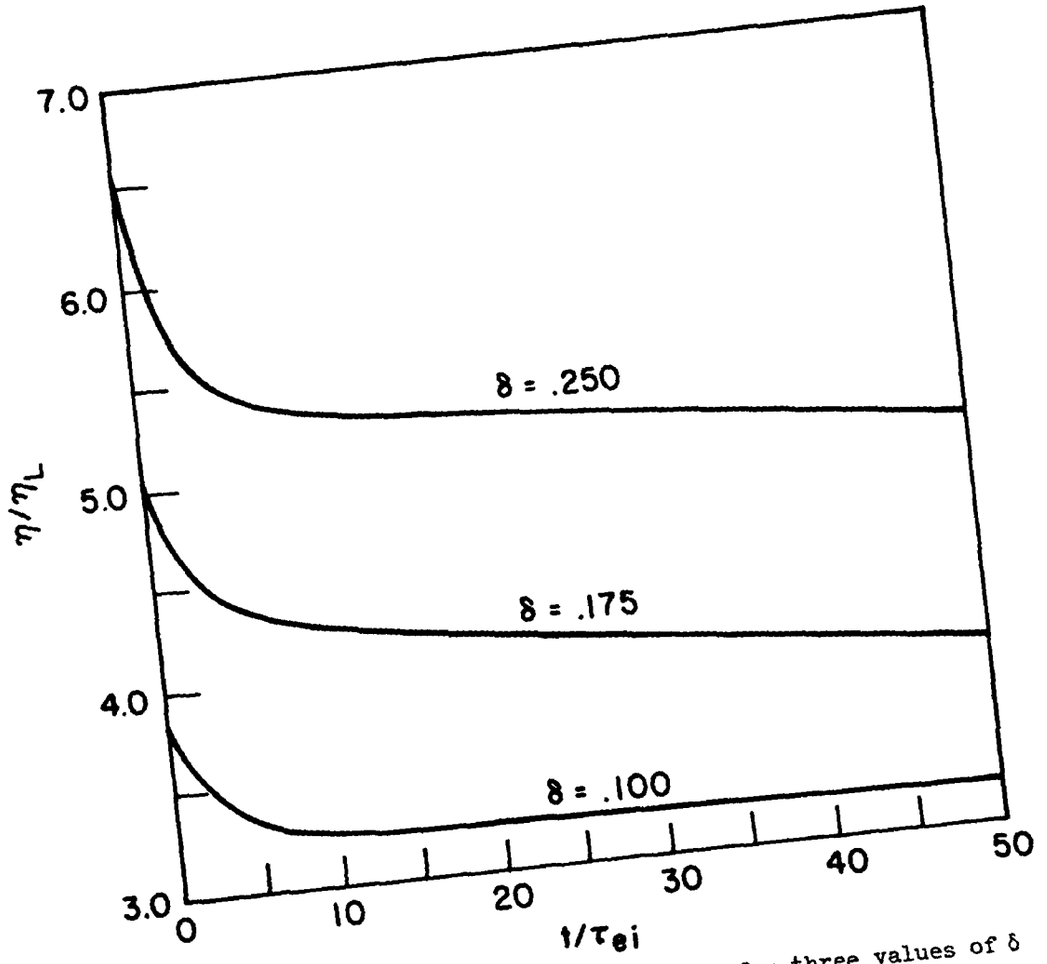

Fig. 9 - The resistivity as a function of time for three values of δ

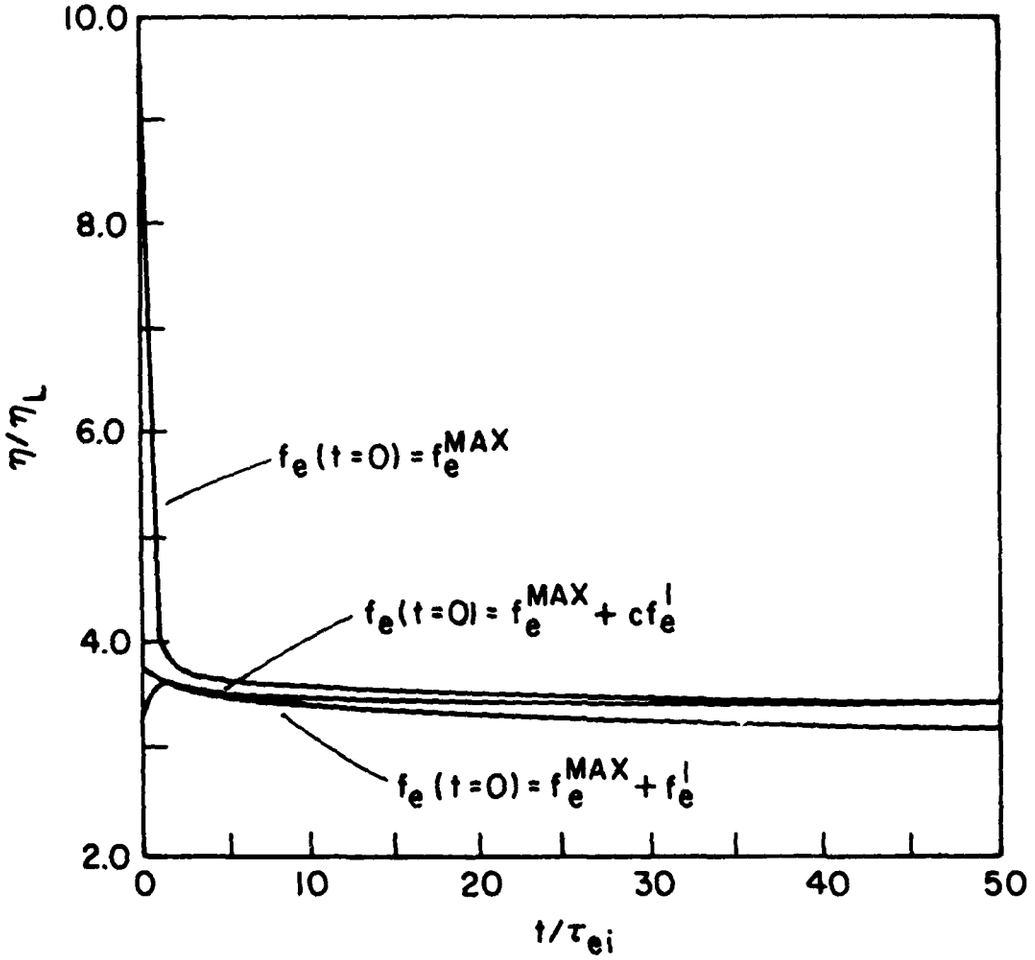

Fig. 10 - The resistivity as a function of time for three different initial distribution functions

In summary, these results confirm the intuitive notions that trapped particle populations inhibit conduction, that the Dreicer field roughly separates situations of approximate quasi-static solutions from those of well developed runaway, and that a Spitzer-Harm type of solution is a good approximation for suitably short times in the weak field case.

ACKNOWLEDGMENT

This work was supported by the Department of Energy under Contract EX-76-A-34-1006.

Appendix A - Details of the Numerical Methods

Equation (28) with the prescribed boundary values and suitable initial data constitutes an initial-value problem for the averaged electron distribution function F(x,y). This section describes the resulting implicit difference equations, and an algorithm for their solution.

Equation (28) has the form

$$\frac{\partial G}{\partial t} = \frac{\partial}{\partial y}(AG) + \frac{\partial}{\partial x}\left[B\frac{\partial G}{\partial x} + CG\right]. \tag{A1}$$

Thus $\int_0^1 \int_0^1 (G^+ + G^- + G^*)\,dxdy$ changes only if the boundary conditions allow a flux through the boundary. This property will be preserved in the numerical algorithm. It can most easily be done if the x and y derivatives in Eq. (A1) are replaced by centered differences.

Let the boundaries of the Cartesian grid be $x = I/N_x$, $I=0..N_x$ and $y = J/Ny$, $J = 0..N_y$. Then the change in G within a grid cell is

$$\frac{\partial}{\partial t} G\,(I+\tfrac{1}{2},\ J+\tfrac{1}{2}) = \frac{1}{\delta x}\left[P\,(I+1,\ J+\tfrac{1}{2}) - P\,(I,\ J+\tfrac{1}{2})\right] + \frac{1}{\delta y}\left[Q\,(I+\tfrac{1}{2},\ J+1)\right.$$

$$\left. - Q\,(I+\tfrac{1}{2},\ J)\right] \tag{A2}$$

in terms of the fluxes through the cell boundaries

$$P\,(I,\ J+\tfrac{1}{2}) = \tfrac{1}{2}\Big\{\left[C(I+\tfrac{1}{2},\ J+\tfrac{1}{2})\,G\,(I+\tfrac{1}{2},\ J+\tfrac{1}{2}) + C(I-\tfrac{1}{2},\ J+\tfrac{1}{2})\,G\,(I-\tfrac{1}{2},\ J+\tfrac{1}{2})\right]$$

$$+ \frac{1}{\delta x}\left[B(I+\tfrac{1}{2},\ J+\tfrac{1}{2})\,G\,(I+\tfrac{1}{2},\ J+\tfrac{1}{2}) - B(I-\tfrac{1}{2},\ J+\tfrac{1}{2})\,G\,(I-\tfrac{1}{2},\ J+\tfrac{1}{2})\right.$$

$$\left. + B(I-\tfrac{1}{2},\ J+\tfrac{1}{2})\,G\,(I+\tfrac{1}{2},\ J+\tfrac{1}{2}) - B(I+\tfrac{1}{2},\ J+\tfrac{1}{2})\,G\ \ (I-\tfrac{1}{2},\ J+\tfrac{1}{2})\right]\Big\} \tag{A3}$$

and

$$Q\,(I+\tfrac{1}{2},\ J) = \tfrac{1}{2}\left[A(I+\tfrac{1}{2},\ J+\tfrac{1}{2})\,G\,(I+\tfrac{1}{2},\ J+\tfrac{1}{2}) + A(I+\tfrac{1}{2},\ J-\tfrac{1}{2})\,G\,(I+\tfrac{1}{2},\ J-\tfrac{1}{2})\right]. \tag{A4}$$

These expressions apply on the interior boundaries of all cells. On the edges of the unit square, the fluxes are zero. On the separatrix, the two

fluxes, P^+ and P^-, both represent transport from the density in the adjacent trapped electron cell, while they add separately to their respective untrapped-electron densities.

The separatrix is most conveniently treated by choosing a in Eq. (10) so that it lies on a grid boundary. In particular, for a physics problem in which both trapped and untrapped electrons are important, and there are no external sources of electrons at some particular energy, the most natural choice of the adjustable grid parameters is

$$a = \frac{B_{max}}{B_{min}} - 2 \qquad (A5)$$

and

$$H_o = kT, \qquad (A6)$$

where T is a representative temperature of interest; e.g., the anticipated thermal electron temperature of the plasma. Cases with $B_{max} < 2B_{min}$ cause no problem, since a appears in Eqs. (25-32) only in the combinations (1+a) and (1+ax). Thus, no poles or zeros are introduced in the unit square provided $a > -1$.

It remains to specify the time difference formulation of Eqs. (A2-A4). It can be most compactly stated in terms of Eq. (A1). A convenient general form is

$$\frac{1}{\delta t}[G(t+1) - G(t)] = (1-s)\frac{\delta}{\delta y}[AG(t)] + (1-s)\frac{\delta}{\delta x}\left[B\frac{\delta G(t)}{\delta x} + CG(t)\right]$$

$$+ s\frac{\delta}{\delta y}[AG(t+1)] + s\frac{\delta}{\delta x}\left[B\frac{\delta G(t+1)}{\delta x} + CG(t+1)\right], \qquad (A7)$$

where G (t+1) represents evaluation of G at time $t + \delta t$. Here $s = 1$ is an explicit algorithm, $s = 0$ is fully implicit, and $s = 0.5$ is an implicit algorithm which is second-order accurate in time.

Suppose the parameters in Eqs. (A5, A6) are used. Then G consists of $\frac{3}{2} N_x N_y$ elements, of which $\frac{1}{2} N_x N_y$ represent G^+, $\frac{1}{2} N_x N_y$ represent G^-, and $\frac{1}{2} N_x N_y$ represent G^*. A grid of this type is shown in Fig. 11. Treating all these elements as a column vector, Eq. (A7) with the space differences expanded according to Eqs. (A2-A4), leads to a matrix equation of the form

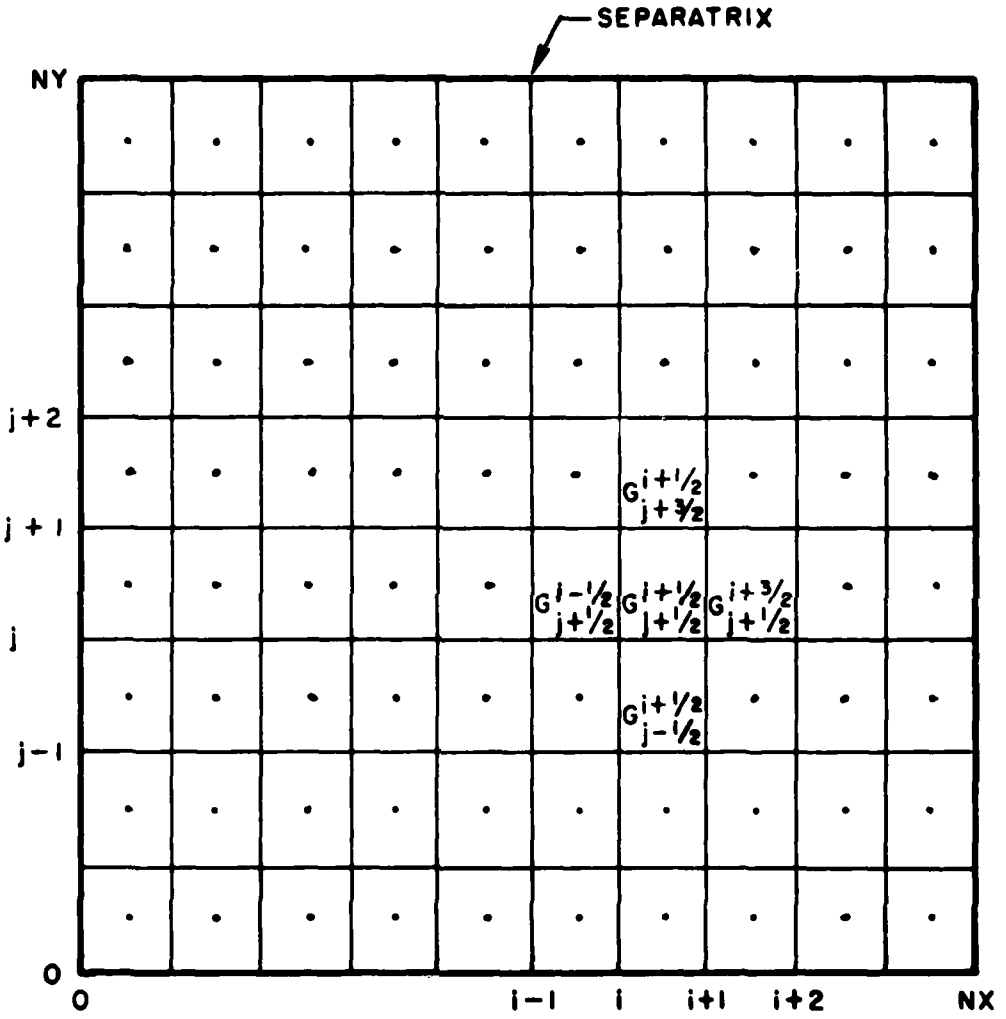

Fig. 11 - Finite difference representation of the problem domain

$$\left(\frac{1}{\delta t}\,\overleftrightarrow{I} - s\,\overleftrightarrow{L}\right) G(t+1) = \left(\frac{1}{\delta t}\,\overleftrightarrow{I} + (1-s)\,\overleftrightarrow{L}\right) G(t). \qquad (A8)$$

Here $\overleftrightarrow{L}$ is the space-difference operator and $\overleftrightarrow{I}$ is the identity matrix. Now the right-hand side can be explicitly calculated, and the left-hand side can be solved by any conventional sparse-matrix equation solver. This is all that is needed to advance the solution of Eq. (13) in time, and the distribution function can be calculated from it by retracing the coordinate transformations.

Appendix B - First Order Correction to the Electron Distribution Function

We desire a quasi-steady solution of Eqs. (20-22) for which the collision term is formally dominant. Seeking a solution of the form given in equation 15 we find the first order equations to be

$$\frac{\partial}{\partial \mu}\left[D\,\frac{\partial f_o^j}{\partial \mu}\right] \quad \text{where } j = +, -, *. \tag{B1}$$

The solution of Eq. (1B) satisfying regularity at $\mu = 0$ and vanishing at inifinity is

$$f_o^j = f_o^j(H).$$

The next order equations can be written

$$\frac{\partial}{\partial \mu}\left[D\,\frac{\partial f_1^{\pm}}{\partial \mu}\right] = \pm\,\Delta\,\frac{\partial f_o^{\pm}}{\partial H} \tag{B2}$$

and

$$\frac{\partial}{\partial \mu}\left[D\,\frac{\partial f_1^{*}}{\partial \mu}\right] = 0 \tag{B3}$$

For trapped electrons the solution is again

$$f_1^* = f_1^*(H)$$

and can be absorbed into f_0^*. For circulating electrons, Eq. (2A) mav be integrated to obtain

$$D \frac{\partial f_1^{\pm}}{\partial \mu} = \pm \Delta \frac{\partial f_o^{\pm}}{\partial H} \mu + c. \qquad B4$$

Since D vanishes as $\mu \to 0$ the constant of integration must be zero. A further integration yields

$$f_1^{\pm} = \pm \Delta \frac{\partial f_o^{\pm}}{\partial H} \int^{\mu} \frac{d\mu' \mu'}{D(\mu')} + c \qquad B5$$

In order to make f_1 continuous on the separatrix the constant of integration is absorbed into the integral form by writing it as a definite integral, i.e.,

$$f_1^{\pm} = \pm \Delta \frac{\partial f_o^{\pm}}{\partial H} \int_{\mu}^{H/B_{MAX}} \frac{d\mu' \mu'}{D(\mu')} \qquad B6$$

Finally we have

$$f^{+} = f_o^{+}(H) + \Delta \frac{\partial f_o^{+}(H)}{\partial H} \int_{\mu}^{H/B_{MAX}} \frac{d\mu' \mu'}{D(\mu')} , \qquad B7$$

$$f^{-} = f_o^{-}(H) - \Delta \frac{\partial f_o^{-}(H)}{\partial H} \int_{\mu}^{H/B_{MAX}} \frac{d\mu' \mu'}{D(\mu')} , \qquad B8$$

$$f^{*} = f_o^{*}(H) , \qquad B9$$

and we have taken $f_o^{+}(H) = f_o^{-}(H) = f_o^{*}(H)$ to be Maxwellian.

References

1. S. Chapman and T. G. Cowling, The Mathematical Theory of Non-Uniform Gases, Cambridge University Press, London, 1939.
2. Lyman Spitzer, Jr., Physics of Fully Ionized Gases, Princeton University Press, 1956.
3. F. L. Hinton and C. R. Oberman, Nuc. Fusion 9, 319 (1969).
4. F. L. Hinton and R. D. Hazeltine, Rev. Mod. Phys. 48, 239 (1976).
5. H. Dreicer, Phys. Rev. 115, 23 (1959) and 117, 329 (1960).
6. W. Bernstein, F. F. Chen, M. A. Heald and A. Z. Kranz, Phys. Fluids 1, 430 (1958).
7. M. D. Kruskal and I. B. Bernstein, Princeton Plasma Physics Laboratory Report MATT-Q-20, 194 (unpub., 1962).
8. A. V. Gurevitch, Zh. Eksp. Teor. Fiz. 39, 1296 (1960) [Sov. Phys. JETP 12, 904 (1961)].
9. A. N. Lebedev, Zh. Eksp. Teor. Fiz. 48, 1393 (1965) Sov. Phys. JETP 21, 931 (1965).
10. J. Killeen and K. D. Marx, in Methods in Computational Physics, ed. B. Alder, et al. (Acad. Press, New York, 1970), Vol. 9, p. 421.
11. R. M. Kulsrud, et al, Phys. Rev. Lett. 31, 690 (1973).
12. B. Coppi, Massachusetts Institute of Technology Report PRR-7417 (1974) see also Proceedings Symposium on Plasma Heating (Editrice Compositori, Bologna, 1976) and A.A.M. Oomens, et al, Phys. Rev. Lett. 36, 255 (1976).
13. P. H. Hui, N. K. Winsor and B. Coppi, Phys. Fluids 20, 1275 (1977).
14. K. Papadopoulos, B. Hui and N. Winsor, Nucl. Fusion 17, 1086 (1977).

15. B. H. Hui and N. K. Winsor, Phys. Fluids 21, 940 (1978).

16. N. K. Winsor, B. H. Hui and B. Coppi, Theory of Magnetically Confined Plasmas (Pergamon Press, New York, 1979), p. 71.

17. A. Airoldi and R. Pozzoli, Proceedings of the Third Symposium on Plasma Heating in Toroidal Devices (Editrice Compositori, 1976) p. 235.

18. R. D. Hazeltine, Plas. Phys. 15, 77 (1973).

19. M. Abramowitz and I. A. Stegun, Eds., Handbook of Mathematical Functions (National Bureau of Standards, Washington, D.C., 1967).

20. M. N. Rosenbluth, R. D. Hazeltine and F. L. Hinton, Phys. Fluids 15, 116 (1972).

DISTRIBUTION LIST

DOE
P.O. Box 62
Oak Ridge, Tenn. 37830

UC20 Basic List (116 copies)
UC20f (192 copies)
UC20g (176copies)

NAVAL RESEARCH LABORATORY
Washington, D.C. 20375

Code 4700 (25 copies)
Code 4790 (150 copies)

DEFENSE TECHNICAL INFORMATION CENTER
Cameron Station
5010 Duke Street
Alexandria, VA 22314 (12 copies)

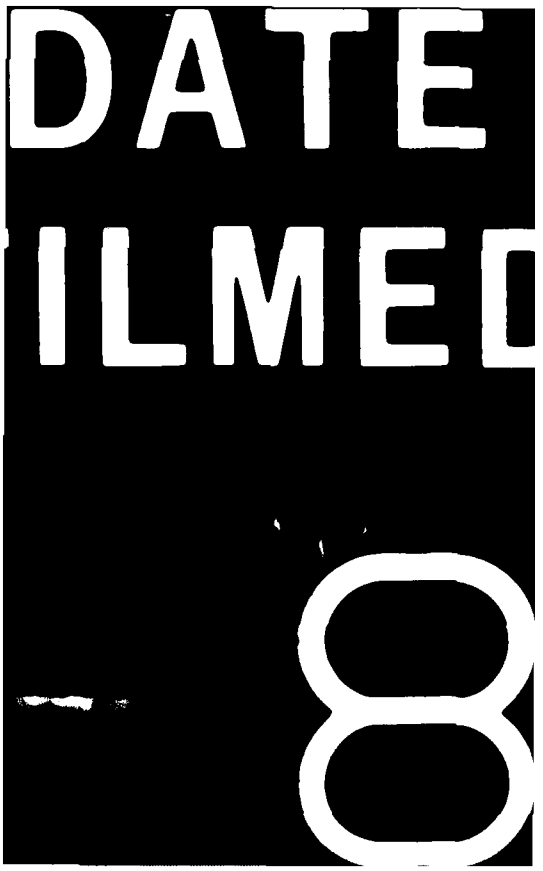
DATE
ILMED
8